Spatial Scales of Kinetic Energy in the Arctic Ocean

Caili Liu[1,2], Qiang Wang[2] , Sergey Danilov[2,3] , Nikolay Koldunov[2], Vasco Müller[2] , Xinyue Li[2], Dmitry Sidorenko[2] , and Shaoqing Zhang[1]

[1]Ocean University of China, Qingdao, China, [2]Alfred Wegener Institute, Helmholtz Centre for Polar and Marine Research (AWI), Bremerhaven, Germany, [3]Jacobs University, Bremen, Germany

Abstract Despite the importance of the Arctic Ocean for the large-scale circulation and climate, there is still a knowledge gap in our understanding of the spatial characteristics of the Arctic Ocean circulation, especially for the mesoscale. This paper investigates the spatial characteristics of the Arctic Ocean circulation using a simulation with 1 km horizontal resolution. We revealed that there are two peaks in the kinetic energy (KE) spectral density at the 400 m depth, one at the gyre scale of the Arctic Circumpolar Boundary Current (centered at 1,700–2,000 km), and the other associated with the mesoscale (at about 60 km). However, at the 70 m depth, the boundary currents tend to mask the spectrum peak associated with the mesoscale. The KE spectrum exhibits a power-law scaling typical for ocean eddies. We found that about 80% (50%) of the KE is on scales smaller than 100 km (30 km). The maximum KE content is in the 10–20 km scale band in most of the eddy-rich regions of the abyssal ocean. The seasonality of the KE spectrum and KE content inside the Arctic Ocean follow the seasonality of eddy activity and baroclinicity, with low values in spring and maxima in late summer to autumn, and the seasonal variation is stronger at the 70 m depth than the 400 m depth. The strong concentration of KE on the very small spatial scales warrants future studies on energy transfer between scales in the Arctic Ocean.

Plain Language Summary We identified the two dominant spatial scales of the Arctic Ocean circulation, the gyre scale of the Arctic boundary currents and the mesoscale, on the energy spectrum of the Arctic Ocean circulation. We found that most of the kinetic energy in the Arctic Ocean is on scales smaller than 100 km, and about half of the kinetic energy is on scales smaller than 30 km. The findings help improve our understanding of the spatial characteristics of the Arctic Ocean circulation and kinetic energy.

1. Introduction

The Arctic Ocean has a strong halocline that insulates the cold mixed layer and sea ice above from the underlying warm Atlantic Water layer (Rudels et al., 1996). The Arctic Circumpolar Boundary Current, as one of the major large-scale circulations in the Arctic Ocean, has an Arctic shelf break branch in the halocline and a Fram Strait branch in the Atlantic Water layer (Aksenov et al., 2011; Karcher & Oberhuber, 2002; Rudels, 2012). The maintenance of the Arctic halocline and the Atlantic Water layer circulation is contributed by mixing induced by mesoscale eddies (Spall, 2013), while eddy formation hotspots in the Arctic Ocean are along the Arctic boundary currents (Kawaguchi et al., 2012; Pickart et al., 2005; Pnyushkov et al., 2018; Spall et al., 2008; Wang et al., 2020; Watanabe et al., 2014).

Available observations, despite being sparse in space and time, indicate that mesoscale eddies are ubiquitous in the Arctic Ocean, including the halocline and the depth range of the Atlantic Water layer (Manley & Hunkins, 1985; Pnyushkov et al., 2018; Timmermans et al., 2008; Woodgate et al., 2001; Zhao et al., 2014, 2016; Zhao & Timmermans, 2015). Some recent studies investigated the role of Arctic Ocean eddies using eddy-permitting or eddy-resolving model simulations (Manucharyan & Thompson, 2022; Meneghello et al., 2021; Regan et al., 2020). Both model simulations and observations indicate that Arctic eddy activity is highest in Fram Strait and along topography slopes inside the Arctic Ocean, including the Eurasian continental slope, the Lomonosov Ridge and the western Arctic continental slope (Wang et al., 2020).

Ocean kinetic energy (KE) is distributed over a wide range of spatial scales, covering large and gyre scales, mesoscale and even smaller scales. Currently there is a lack of understanding of the spatial scales of Arctic Ocean KE, and in general there is a great challenge in studying the mesoscale in the Arctic Ocean. Firstly, there are no sufficient observations of eddies in the Arctic due to sea ice cover and very limited instruments (von Appen et al., 2022). The issue of data scarcity is further complicated by the small horizontal scales of mesoscale dynamics in high-latitude regions, with the first baroclinic Rossby radius of deformation around 7–15 km in the

Validation: Caili Liu, Qiang Wang,
Sergey Danilov, Vasco Müller, Xinyue Li
Visualization: Caili Liu,
Nikolay Koldunov, Xinyue Li
Writing – original draft: Caili Liu,
Qiang Wang, Sergey Danilov,
Shaoqing Zhang
Writing – review & editing: Caili Liu,
Qiang Wang

Arctic (Nurser & Bacon, 2014; Timmermans & Marshall, 2020). Secondly, the resolution used in long model simulations is usually not fine enough to resolve mesoscale dynamics in the Arctic Ocean. Decade-long eddy-resolving simulations with 1 km resolution became available only recently (Wang et al., 2020).

Multiscale ocean dynamics can be investigated through decomposing KE on spatial scales. Although KE spectrum analysis has been widely used to study the global ocean, successfully revealing properties that are not easily discernible from raw data (e.g., Ferrari & Wunsch, 2009; Klein et al., 2008; Qiu et al., 2018; Storer et al., 2022), similar analysis was not performed for the Arctic Ocean circulation yet. Scale decomposition of the global ocean circulation using a coarse-graining method successfully revealed the spectral energy density and the energy distribution in scale bands for both a 1/12°-resolution model simulation and the 1/4°-resolution satellite observations (Storer et al., 2022). However, mesoscale eddies in the Arctic Ocean are not well resolved with a model resolution of 1/12°, and not captured by the satellite observations at a resolution of 1/4°. Therefore, the spatial characteristics of KE in the Arctic Ocean remain unknown.

To fill the knowledge gap mentioned above, we use a decade-long eddy-resolving model simulation to investigate the characteristics of KE in the Arctic Ocean in this paper. We analyze the energy spectrum of the ocean circulation, quantify the energy content in different spatial-scale bands, and study how the KE spectrum and KE content change at different spatial locations and in different seasons. We focus on the halocline and Atlantic Water layer in this paper. For the first time we revealed two peaks in the spectral energy density for the Arctic Ocean, associated with the gyre-scale Arctic Ocean boundary currents and mesoscale eddies, respectively. We also found that most of the KE is on spatial scales smaller than 100 km in the Arctic Ocean.

The rest of this article is organized as follows. Section 2 presents the methodology of data analysis and the model simulation. In Section 3, we explore the energy spectrum as the function of spatial scales and the KE content in different scale bands. Finally, in Section 4, we summarize the results.

2. Data and Methodology

2.1. Model Simulation at 1 km Resolution

The model data used here is from the Finite-Element/volumE Sea ice-Ocean Model version2 (FESOM2) simulation. FESOM2 is a multi-resolution sea ice-ocean model that solves the ocean primitive equations on unstructured meshes (Danilov et al., 2017). Its sea ice module is formulated on the same unstructured meshes as the ocean (Danilov et al., 2015). FESOM2 can reasonably represent the global ocean and sea ice (Koldunov et al., 2019; Scholz et al., 2019, 2022; Wang et al., 2024).

The model configuration has horizontal resolutions of 1 km in the Arctic and 30 km in the rest of the global ocean. In the vertical it has 70 z-levels with 5-m spacing in the upper 100 m. It is driven by the atmospheric reanalysis fields from ERA5 (Hersbach et al., 2020). Free-slip boundary condition was used at the ocean boundary. The simulation was initialized from the PHC3 climatology (Steele et al., 2001) starting from 2010 and has been run for 11 years. The first 4 years are considered model spinup and the last 7 years (2014–2020) are analyzed in this study. The snapshots of ocean current speed and relative vorticity in Figure 1 obtained from this model simulation clearly indicate the eddy activities in the Arctic Ocean, with a spatial pattern consistent with previous studies (Wang et al., 2020; von Appen et al., 2022).

The Arctic Ocean in this study is defined as the region north of 77°N in the Fram Strait, east of 20°E in the Barents Sea Opening, and north of the Bering Strait, which has 1 km horizontal resolution (inset in Figure 1a).

2.2. Coarse-Graining Method

We employ the coarse-graining method proposed by Aluie (2019) to study the spatial scales of the Arctic Ocean circulation. This method has been successfully applied to understand the multiscale dynamics of the ocean (Aluie et al., 2018; Rai et al., 2021; Sadek & Aluie, 2018; Schubert et al., 2020; Storer et al., 2022). Coarse-graining can be considered a "blurring" process (analogized with taking off one's glasses to have a blurrier picture) (Storer et al., 2022). Mathematically, its main idea is to apply a low-pass filter with a convolution approach.

First, we define the convolution kernel G centered at point $\mathbf{x}$ for the scale ℓ,
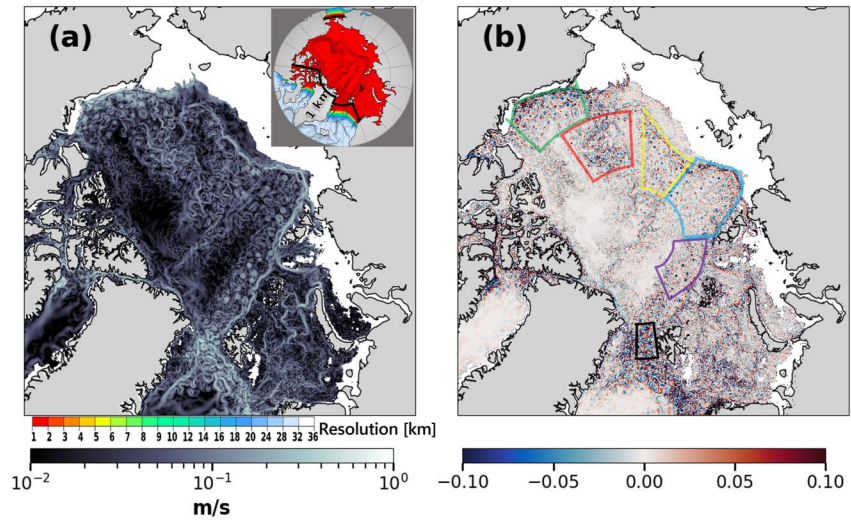
Figure 1. Eddies are ubiquitous in the Arctic Ocean. A snapshot on 1 October 2017 from FESOM2 1 km-resolution simulations: (a) ocean current speed at 70 m depth and (b) Rossby number at the same depth. Several regions of high eddy activity studied in this paper are denoted by boxes in (b), including Fram Strait (black), central Nansen Basin (purple), east Eurasian Basin (blue), Makarov Basin (yellow), Chukchi Borderland (red) and Beaufort Sea (green). Note that 1 km resolution is only applied inside the Arctic Ocean in the global simulation. The inset in (a) shows the horizontal resolution and the locations of the Arctic boundary defined in this study.

$$G_\ell(\mathbf{r}) = \frac{A}{2}[1 - \tanh((|\mathbf{r}| - \ell/2)/S_t)], \tag{1}$$

where $|\mathbf{r}|$ is the geodesic distance from the point $\mathbf{x}$, the transition scale $S_t = 2$ km, and A is the normalization factor that guarantees $\sum G_\ell(r) = 1$ (where the sum is over all the elements of the matrix) (Aluie, 2019; Rai et al., 2021).

Then one can obtain the low-pass filtered field $\overline{\varphi}$ after the convolution operation (*) over the original field φ as

$$\overline{\varphi}_\ell = G_\ell * \varphi. \tag{2}$$

$\overline{\varphi}_\ell$ contains length scales larger than ℓ.

$G_\ell(\mathbf{r})$ is expected to be uniform when $|\mathbf{r}|$ is smaller than $\ell/2$ and smoothly decrease to zero when $|\mathbf{r}|$ approaches $\ell/2$. As we will calculate the coarse-grained field $\overline{\varphi}_\ell$ at scales as small as a few kilometers, the value of S_t is chosen to be small as well.

Before the coarse-graining is performed, we transformed the spherical coordinate so that the Arctic Ocean is centered at the equator. That is, in the new coordinate, the equator crosses the center of the Arctic Ocean, and the Arctic Ocean spans a latitude range of about ±20 . In this case, we can coarse-grain the two velocity components separately, with the spherical effect, the impact of the metric term, neglected. When analyzing a large domain such as the global ocean or studying energy transfer across scales, one needs to employ Helmholtz decomposition before performing convolution (Aluie, 2019), or use implicit filters by solving Laplacian equations formulated in spherical coordinates (Danilov et al., 2024).

2.3. Kinetic Energy Spectrum and Content

After obtaining the coarse-grained velocity $\overline{\mathbf{u}}_\ell$ from daily velocity fields, the coarse KE contained in scales larger than ℓ is calculated as

$$\mathcal{E}_\ell = \frac{1}{2}|\overline{\mathbf{u}}_\ell(\mathbf{x}, t)|^2. \tag{3}$$
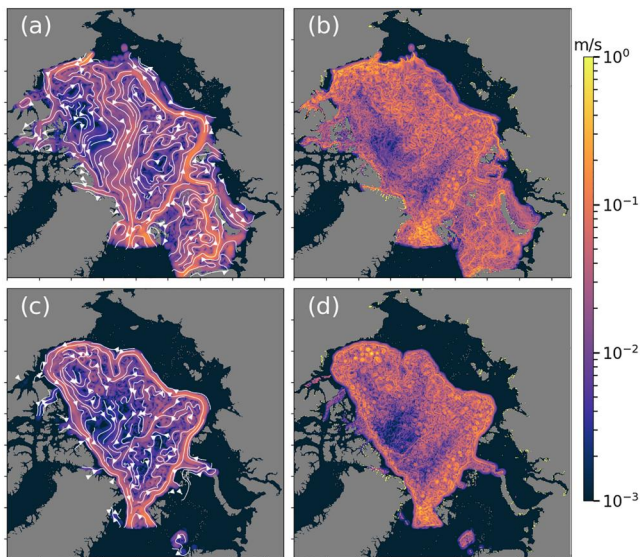
Figure 2. Gyre-scale and mesoscale flows of the Arctic Ocean for the day on 01 October 2017 obtained from the coarse-graining method. Velocity magnitude for (a) spatial scales larger than 100 km and (b) smaller than 100 km at 70 m depth. (c) and (d) are same as (a) and (b), but at 400 m depth. White contours in (a) (c) denote the streamlines of the coarsened velocity, with arrows showing the direction of the flow.

Following Sadek and Aluie (2018), one can then obtain the spectral energy density, a quantity similar to the power spectral density (PSD) obtained from Fourier analysis, by differentiating the coarse KE with respect to length scale:

$$\overline{E}(k_\ell, t) = \frac{\mathrm{d}}{\mathrm{d}k_\ell}\{\mathcal{E}_\ell\} = -\ell^2 \frac{\mathrm{d}}{\mathrm{d}\ell}\{\mathcal{E}_\ell\}, \tag{4}$$

where $k_\ell = 1/\ell$ is the filtering wave number and $\{\cdot\}$ denotes spatial averaging. As shown in Storer et al. (2022), $\overline{E}(k_\ell, t)$ is equivalent to the traditional Fourier spectrum when applying Fourier analysis is possible. In comparison to Fourier analysis, the coarse-graining method has the advantage to be also able to provide the spatial distribution of the coarse-grained fields (such as Figures 2 and 5 that we will show below).

Land areas are treated in the same way as in Storer et al. (2022), with velocity in land cells set to zero and coarse-grained like water cells. In the spatial averaging in Equation 4, the coarse KE on all grid cells is summed, including land cells, and divided by the total area of water cells. That is, the cell area on the denominator contains only the water area. In this case, there is no loss of KE in the analysis. The treatment is merely a normalization choice and does not affect our findings. One can refer to Storer et al. (2022) for further in-depth discussions about treatment of land areas.

The KE contained in a scale band between scales ℓ_1 and ℓ_2 can be obtained via

$$\mathrm{KE}_{[\ell_1,\ell_2]}(\mathbf{x}, t) = \mathcal{E}_{\ell_1} - \mathcal{E}_{\ell_2}. \tag{5}$$

3. Results

3.1. Kinetic Energy Spectrum and Power Spectral Density Peaks

In this study, we focus on the 70 and 400 m depths, representing the upper halocline and the Atlantic Water layer, respectively. The upper depth is consistent with the typical core depths of eddies in the halocline observed by mooring instruments and Ice Tethered Profilers (Zhao & Timmermans, 2015; Zhao et al., 2014, 2016). The warm Atlantic water layer is located in the depth range of approximately 150–800 m, with maximum temperature in the depth range of 200–400 and 400–600 m in the Eurasian Basin and Amerasian Basin, respectively (Wang et al., 2024). Therefore, we choose 400 m depth to represent the Atlantic Water layer in our analysis.

Figure 2 shows an example of applying coarse-graining to the velocity at 70 and 400 m depths on 1st October 2017. The used filter scale is 100 km. The low-pass filtered velocity (Figures 2a and 2c) depicts the large-scale circulation in the Arctic, including the inflow through Fram Strait and the Barents Sea in the Atlantic sector, the cyclonic circumpolar boundary current along the continental slope, and the return flow along the Lomonosov Ridge, consistent with what we know about the Arctic Ocean circulation (Aksenov et al., 2011; Karcher & Oberhuber, 2002; Rudels, 2012; Timmermans & Marshall, 2020; Wang & Danilov, 2022). Meanwhile, the fine-scale velocity $\mathbf{u}' = \mathbf{u} - \overline{\mathbf{u}}_{\ell=100\mathrm{km}}$ (Figures 2b and 2d) presents the flows at the scales smaller than 100 km. In the deep basin area, the fine-scale flows are dominated by mesoscale eddies in the vicinity of continental slopes in both the western and eastern Arctic, over the Chukchi Borderland and along the Lomonosov Ridge off the Siberian continental shelf, consistent with the eddy field shown by relative vorticity on the same day (Figure 1b). The above example illustrates the success of the method in separating the flow spatial scales. Note that, in the Barents Sea, the first baroclinic Rossby radius is smaller than in the deep basin (Nurser & Bacon, 2014; Timmermans & Marshall, 2020) and 1 km resolution might be insufficient for fully resolving mesoscale eddies.

As shown in Figure 3, the KE spectral scaling for both the 70 m depth and the 400 m depth lies between $k^{-5/3}$ and k^{-3} for wavenumbers larger than 3×10^{-2} km^{-1} (i.e., smaller than about 30 km in scales), a typical power-law scaling range at mesoscales and smaller scales in the geophysical flow (Ferrari & Wunsch, 2009). In lower
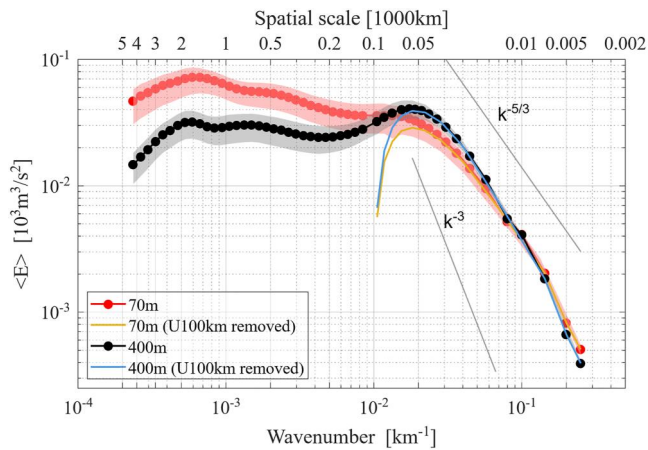
Figure 3. Kinetic energy (KE) spectrum for the Arctic Ocean at 70 m (red) and 400 m (black) depths. The KE spectra are also computed from the fine velocity after removing velocity coarser than 100 km scale, as shown by orange and blue lines for the two depths. The results are averaged over 7 years (2014–2020). Shading colors are inter-quartile range (25th–75th percentiles) of temporal variation. The two gray lines indicate the slopes of $k^{-5/3}$ and k^{-3}, respectively.

latitudes, however, such a power-law scaling is present typically at spatial scales smaller than about 250 km as revealed in previous studies (e.g., Storer et al., 2022; Uchida et al., 2017). The difference between the Arctic Ocean and lower latitudes reflects smaller eddy size in the Arctic Ocean, which is due to the small baroclinic Rossby radius of deformation (Nurser & Bacon, 2014; Timmermans & Marshall, 2020). Furthermore, the Arctic eddies are often not generated through the first mode of baroclinic instability and some eddies could be even smaller than what can be expected from the first baroclinic Rossby radius (Meneghello et al., 2021).

At 70 m depth, the spectrum increases from small spatial scales toward large spatial scales and there is no clear mesoscale peak (Figure 3, red line). On the contrary, for the 400 m depth, there is a spectrum peak centered at the scale of about 60 km (Figure 3, black line). Observations revealed that mesoscale eddies in the Arctic Ocean have a mean diameter of about 10 km (Kozlov et al., 2019; Zhao & Timmermans, 2015). Therefore, the spatial range covering the location of the spectrum peak, from 30 to 100 km, represents the upper bound of the mesoscale in the Arctic Ocean, not the typical size of predominant mesoscale eddies.

When we applied the coarse-graining method to analyze different small regions in the Arctic Ocean with boundary currents along continental slopes excluded from the analysis, we found that all the obtained energy spectra possess mesoscale peaks at the spatial scale of approximately 60 km for the 70 m depth (see Section 3.4). This implies that it is the inclusion of the boundary currents when analyzing the whole Arctic domain that masks the mesoscale peak for the 70 m depth in Figure 3. When the boundary currents are relatively strong as they are at the 70 m depth (Figure 2a), the KE spectrum does not drop from 60 to 200 km (Figure 3, red line). At 400 m depth on the other hand, the boundary currents are relatively weaker, so the mesoscale peak is visible in the KE spectrum (Figure 3, black line).

As we can see in Figures 2b and 2d, after removing the velocity coarsened at 100 km, the remaining velocity is dominated by eddies and filaments. We therefore also calculated the KE spectrum by first removing velocity coarser than 100 km. In this case, spectrum peaks are present for both depths and located at about 60 km (Figure 3, orange and blue lines). Removing velocity coarsened at 100 km before analyzing the spectrum effectively eliminates the impact of boundary currents during the coarse-graining. We note that the exact information on the location of spectrum peaks associated with mesoscale eddies should rely on analysis performed for small regions excluding boundary currents as we did in Section 3.4. Our test here by removing the velocity coarsened at 100 km serves as an illustration about the impact of boundary currents on the spectrum. The fact that the obtained peaks are located at 60 km, the same as the results of analysis for small regions, indicates that the energy associated with boundary currents is largely removed with the choice of the scale of 100 km. This choice was made to have results consistent with analysis of small regions shown in Section 3.4.

The KE spectrum has another peak in the range of 1,700–2,000 km for both the depths considered (Figure 3). This scale can be considered the mean gyre scale of the Arctic-wide boundary currents. Being able to reveal both the mesoscales and gyre scales in the KE spectrum is one of the advantages of the coarse-graining method (Storer et al., 2022). However, as shown above, the spectrum peak representing the upper bound range of mesoscales is rather absent for the Arctic flow at the 70 m depth due to the relatively strong boundary current and relatively weak eddy intensity in the Arctic. This issue is not present for lower latitudes where eddy intensity is relatively high (Storer et al., 2022).

3.2. Kinetic Energy Content in Scale Bands

Figure 4 shows that the scales smaller than 10 km contains the highest KE among all the 10 km scale bands for the 70 m depth, while the 10–20 km band has the highest KE at the 400 m depth. On scales larger than 20 km, the KE content decreases with the increase in the scales for both the depths considered. At the 70 m depth, 47% of the total KE is contained in the scale band smaller than 30 km, 22% in the scale band of 30–60 km, 12% in the scale band of 60–100 km, and the remaining 19% in all scales larger than 100 km. The KE content distribution for the 400 m
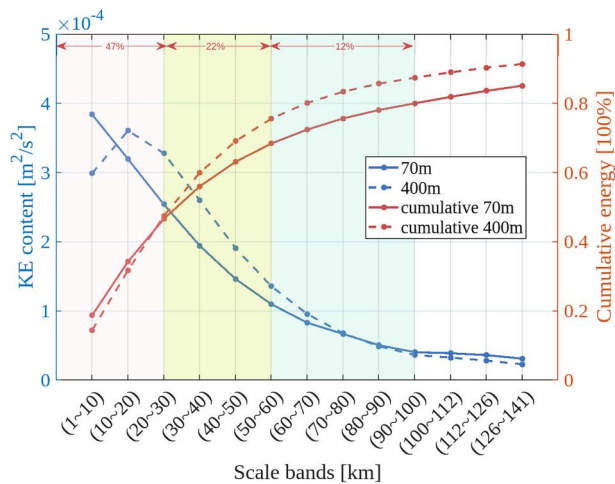
Figure 4. Kinetic energy (KE) content in different spatial-scale bands for 70 m depth (solid blue line) and 400 m depth (dashed blue line). The respective cumulative energy contents (in percentage) are also shown in red lines with y-axis on the right side. The KE contained in the scale bands of 1–30 km, 30–60 km, and 60–100 km for 70 m depth is indicated on the top of the plot. Note that the scales bins are 10 km wide below 100 km and go higher beyond. The result is averaged over 7 years (2014–2020).

depth similarly shows that more than 80% of the KE is contained in scales smaller than 100 km and nearly 50% in scales smaller than 30 km.

With the traditional method such as Fourier analysis, one only gets spectrum plots like our Figure 3. One major advantage of the coarse-graining method is that it preserves the 2D information of the filtered fields and thus allows us to analyze maps of KE contained in different scale bands as defined in Equation 5. The result is shown in Figure 5. In the three scale bands below 100 km, KE is mainly distributed in the vicinity of the circumpolar boundary current and Lomonosov Ridge, and over the Chukchi Borderland, consistent with the spatial distribution of eddies (Figures 1 and 2). These are the regions where previous studies have shown high conversion from eddy available potential energy to eddy kinetic energy (Wang et al., 2020). Figure 4 shows that the KE content in the three scale-bands decreases with the increase in the scale. Figure 5 further demonstrates that this relation applies to all the areas with high KE content. In the scales above 100 km, the highest KE is associated with the main currents. The KE spatial distributions in each scale-band are similar between the two ocean depths.

3.3. Seasonality of Kinetic Energy Spectrum and Content

There is a clear seasonal variation in the KE spectrum at the 70 m depth (Figure 6a). The spectrum value is lower in spring and higher in late summer to autumn for all wavenumbers larger than 10^{-2}. Accordingly, the slope of the spectrum is steeper from late summer to autumn. The spectrum peak is located at about 60 km all year round. At the 400 m depth, the seasonal variation in the KE spectrum has a phase similar to the 70 m depth, but with a clearly smaller magnitude. The fact that the spectrum peak is located in the same period (September–October) for all spatial scales (Figure 6a) indicates that there is no clear spectral lag time inside the Arctic Ocean, different from what was found for the lower latitudes of the global ocean (Storer et al., 2022). The exact reasons for the spectral lag time in the global ocean is not yet fully understood (Storer et al., 2022) and the difference of the Arctic Ocean also remains an open question.

The KE content in different scale bands has a seasonal variation phase similar to that of the KE spectrum, and the magnitude of the seasonal variation is much stronger at the 70 m depth than at the 400 m depth (Figure 6b). In all months, the KE content is the highest in the scale band of 10–20 km at the 400 m depth and in the scale band of 1–10 km at the 70 m depth, and further decreases with the increase in the scales.

The seasonal variation in the KE spectrum and content is consistent with that of the EKE in the halocline and Atlantic Water layer of the Arctic Ocean (von Appen et al., 2022; Wang et al., 2020), which can be attributed to the seasonal variation in the conversion rate from eddy available potential energy to EKE (Wang et al., 2020). Sea ice cover can dissipate existing eddies and prevent the growth of eddies, so the seasonal variation of EKE in the upper few tens of meters is expected to follow the seasonal changes in sea ice cover (Meneghello et al., 2021). However, for ocean depth below about 50 m, the direct impact of sea ice on eddy activity is small, so the variability of EKE is largely determined by the baroclinic energy conversion rate. Therefore, the seasonal variation of the KE spectrum and content for the two depths considered here is not correlated with sea ice cover seasonal changes.

3.4. Kinetic Energy Spectra and Contents in Eddy-Rich Regions

The seasonal variability of KE spectrum and content at 70 m depth is shown in Figure 7 for six eddy-rich regions, including Fram Strait (the deepest Arctic Ocean gateway) and five regions inside the Arctic Ocean. The locations of the six regions are shown in Figure 1b. For these regions, the spectrum peak is similarly located at the scale of about 60 km, and the spectral scaling lies between $k^{-5/3}$ and k^{-3} for wavenumbers larger than 3×10^{-2} km^{-1} (Figure 7, left column). These properties are the same as the Arctic-wide mean properties (Figure 3). The spectrum magnitudes are different among the regions, with the Beaufort Sea region showing the largest magnitude inside the Arctic, exceeded only by the spectrum magnitude in Fram Strait. Note that, we don't need to
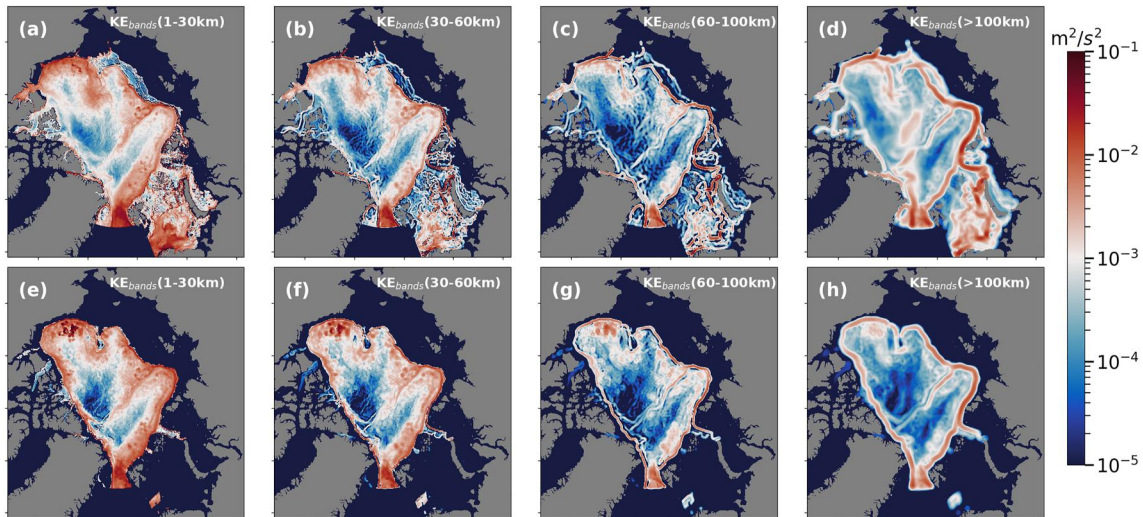
Figure 5. Spatial distribution of KE in different scale bands following Equation 5 at 70 m depth (a–d) and 400 m depth (e–h). The result is averaged over 7 years (2014–2020).

remove the velocity coarser than 100 km when doing coarse-graining for the selected subdomains, as we strategically excluded the boundary currents in the analysis of subdomains.

The seasonal variability of the KE spectrum at 70 m depth in the five eddy-rich regions inside the Arctic Ocean is similar, with low values in spring and the maximum located in late summer to autumn as in the Arctic-wide mean seasonality (Figure 7, middle column). In the Fram Strait, the KE spectrum seasonality is different from that inside the Arctic Ocean. Here, the maximum spectrum peak value occurs in winter, consistent with the seasonality of the EKE in this region, which is elevated by increased baroclinic instability associated with the increase in mixed layer depth in winter (von Appen et al., 2016; Wekerle et al., 2017, 2020).

The KE content shows a seasonality similar to that of the KE spectrum (Figure 7, right column). In most regions, the KE content has a maximum in the 10–20 km scale band and decreases with the increase in the spatial scale.
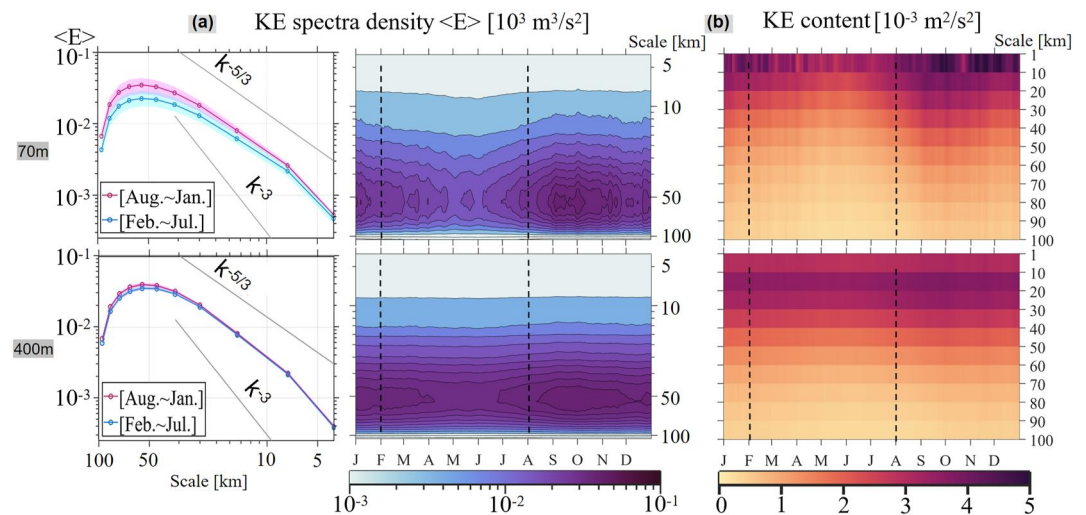
Figure 6. Seasonal variability of (a) kinetic energy (KE) spectrum and (b) KE content for the 70 m depth (upper row) and 400 m depth (lower row). In (a), both the seasonal-mean KE spectrum (left) and the annual cycle of the KE spectrum (right) are shown. The pink shading and blue shading in the KE spectrum denote the standard deviation for the corresponding months. The black dashed lines in the plot of the annual cycle indicate the beginning of February and August, respectively. The results are the average over 7 years (2014–2020).
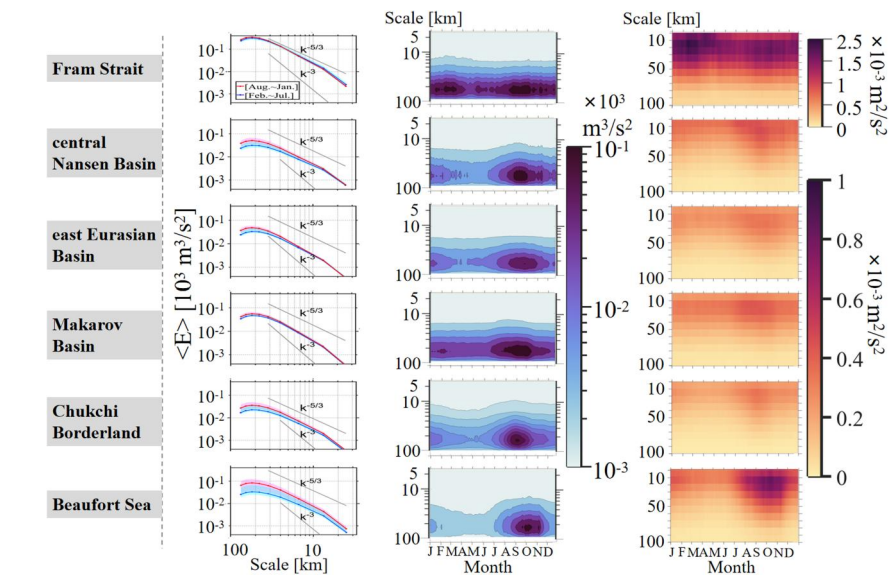
Figure 7. Kinetic energy (KE) spectrum and content for the 70 m depth in 6 regions with high eddy activity. (left) KE spectrum separately for two seasons: August–January and February–July. (middle) Annual cycle of KE spectrum. (right) Annual cycle of KE content in scale bands. The locations of the regions are denoted in Figure 1b. The results are the averages over 7 years. In the right column, the upper colorbar is only for the Fram Strait (the first row), and the lower colorbar is for all other panels.

The KE content better illustrates that the Fram Strait has a maximum in winter, different from the regions inside the Arctic. And the Beaufort Sea has larger KE content than other regions inside the Arctic for all shown scales.

For the 400 m depth level, the properties of the power spectrum (power-law scaling and location of the peak) and its seasonality phase are very similar to those at the 70 m depth (Figure 8). However, the seasonal variations of both the KE spectrum and content are much weaker than at the 70 m depth, consistent with the weaker seasonality in eddy generation and EKE at depth (Wang et al., 2020). The KE content in different scale bands is higher at the 400 m depth than at the 70 m depth in the Eurasian and Makarov basins and in the Beaufort Sea, indicating that the eddy activity in the Atlantic Water layer in these regions is high in the studied period.
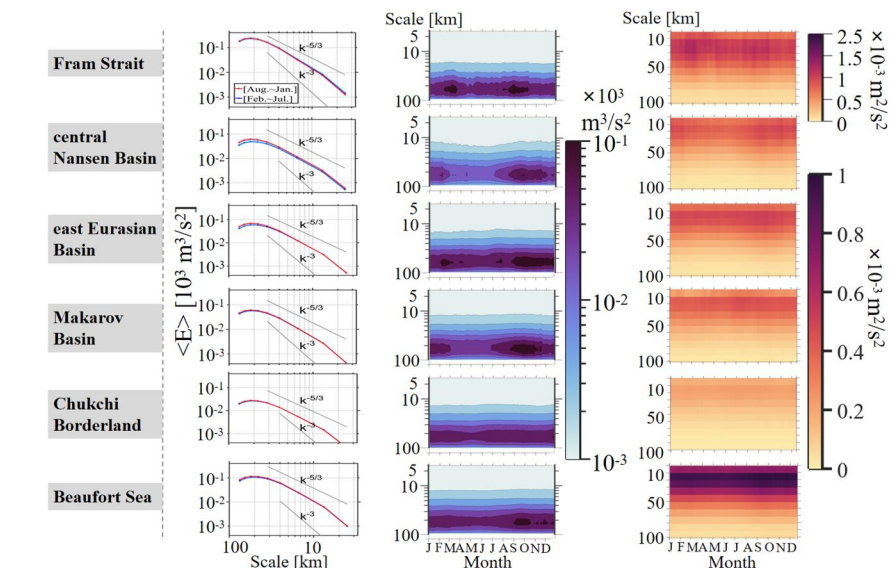
Figure 8. Same as Figure 7, but for the 400 m depth.
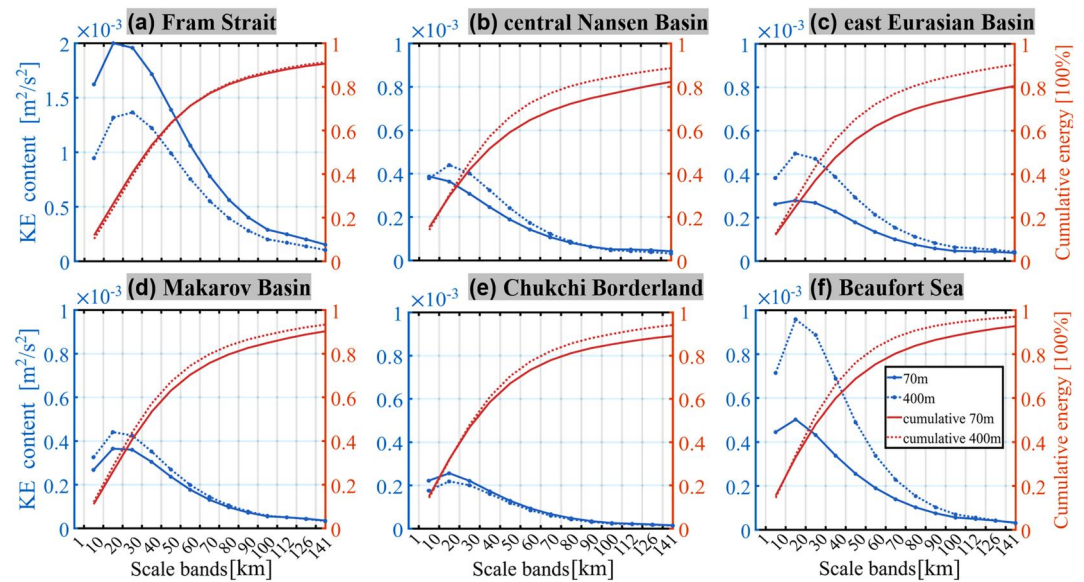
Figure 9. Kinetic energy (KE) content in scale bands in six eddy-rich regions for the 70 m depth (solid blue lines) and 400 m depth (dotted blue lines). The cumulative energy contents (in percentage) are also shown for the 70 m depth (solid red lines) and 400 m depth (dotted red line) with y-axis on the right side. The results are averaged over 7 years (2014–2020). Note that the y-axis range for the Fram Strait in (a) is different from other panels.

The KE contents averaged over each region clearly indicate that the maximum is in the 10–20 km band for both ocean depths and in most regions, expect for the 70 m depth level in the central Nansen Basin (Figure 9). On the contrary, the mean KE content averaged over the whole Arctic Ocean shows that the maximum is located in the 1–10 km band at 70 m depth (Figures 4 and 6b). The reason is that there are large areas where the KE content maximum is located in the 1–10 km band, including the Barents-Kara seas and the central Nansen Basin. In particular, when excluding the Barents-Kara seas, the mean KE content becomes similar between the 1–10 km band and 10–20 km band (Figure 10). This is consistent with the fact that Rossby radius in the shelf seas is smaller than in the abyssal ocean. The cumulative KE in scale bands in different regions similarly shows that about 50% of the KE is on the scales smaller than 30 km and about 80% of the KE is on the scales smaller than 100 km (Figure 9), consistent with the Arctic mean KE content (Figure 4).
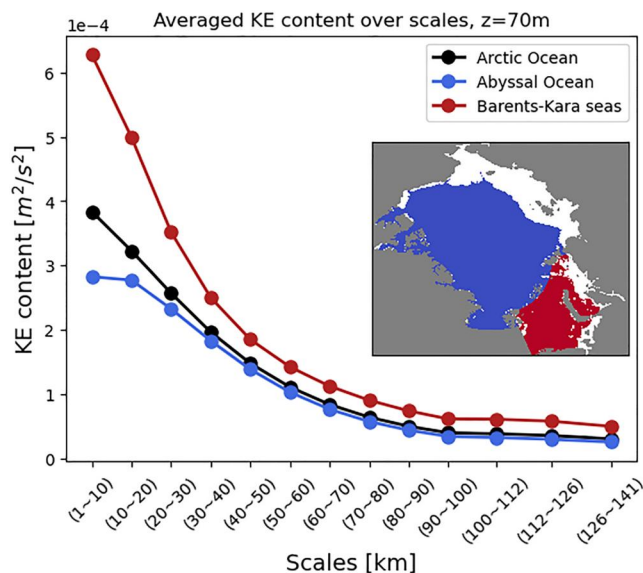
Figure 10. Kinetic energy (KE) content in scale bands for the 70 m depth. The results for the whole Arctic Ocean (black), the abyssal ocean (blue) and the Barents-Kara seas (red) are shown separately. The results are averaged over 7 years (2014–2020). The inset indicates different Arctic regions.

4. Summary

In this paper we applied the coarse-graining method to study the spatial scales of the Arctic Ocean circulation and KE at two ocean depths. Satellite observations and typical high-resolution simulations cannot resolve mesoscale eddies in the Arctic Ocean, so there was a knowledge gap in the understanding of the spatial characteristics of the Arctic Ocean circulation. By using a novel decade-long global simulation with 1 km horizontal resolution in the Arctic Ocean, we filled the knowledge gap in this paper.

Our result shows that the KE spectrum of the Arctic Ocean circulation at 70 m depth has one peak at the scale of about 1,700–2,000 km, which is the gyre scale of the Arctic Circumpolar Boundary Current. The KE spectrum at 400 m depth has two peaks, one at the same scale as the 70 m depth corresponding to the large-scale circulation, the other is centered at 60 km, roughly representing the upper bound of the mesoscales in the Arctic Ocean. The reason for missing the spectrum peak associated with the mesoscale at the 70 m depth is that the boundary current is relatively strong compared with the eddy velocity. Indeed, when analyzing different small regions for the 70 m depth with

boundary currents excluded, we can get a spectrum peak at 60 km, similar to the 400 m depth. The KE spectrum exhibits a similar power-law scaling typical for ocean eddies for both the considered depths.

We found that about 80% of the KE is on the scales smaller than 100 km and about 50% of the KE is on the scales smaller than 30 km at the two depths of the Arctic Ocean. The high concentration of KE on the very small spatial scales is consistent with observed small size of eddies in the Arctic Ocean (Zhao et al., 2014). When separating the KE into scale bands of every 10 km, the maximum KE content is in the 10–20 km band for both the 70 and 400 m depths in most of the Arctic eddy-rich regions. However, because the maximum KE is in the scale band of 1–10 km in some regions such as the Barents-Kara seas, averaged over the whole Arctic Ocean, the maximum KE content is in the 1–10 km band for the 70 m depth.

The seasonality of the KE spectrum and KE content is similar inside the Arctic Ocean in the five eddy-rich regions we analyzed. It follows the seasonality of EKE and baroclinicity, with low values in spring and maximum in late summer to autumn. The maximum magnitude of the KE spectrum and the maximum KE content in the Fram Strait are in winter, when eddy activity is the strongest (von Appen et al., 2016; Wekerle et al., 2017). The seasonal variation is stronger at the 70 m depth than the 400 m depth, consistent with that the conversion rate from eddy available potential energy to EKE has a weaker seasonal variability at depth as found before (Wang et al., 2020).

In this paper, we studied the spectrum and spatial scales of the KE and their seasonal cycle in the Arctic halocline and Arctic Atlantic Water layer. We found that KE in the Arctic Ocean is strongly concentrated on very small scales, while the ocean receives energy from winds on large spatial scales (Rai et al., 2021). Therefore, energy transfer between scales, interaction between surface mixed layer and eddies, and vertical energy fluxes through the water column need dedicated studies in future work. Our decade-long simulation is still relatively short, which does not allow us to study trends in eddy activity associated with the ongoing climate change. Long historical simulations to be carried out in the future will allow us to look into changes in eddy properties and KE spatial scales over the past few decades when the Arctic Ocean physical environment experienced dramatic changes.

Data Availability Statement

The data and the scripts that used to produce the figures in the paper are available at Liu et al. (2024) (https://doi.org/10.5281/zenodo.7895619).

References

Aksenov, Y., Ivanov, V. V., Nurser, A. J. G., Bacon, S., Polyakov, I. V., Coward, A. C., et al. (2011). The Arctic circumpolar boundary current. *Journal of Geophysical Research*, *116*(C9), C09017. https://doi.org/10.1029/2010JC006637

Aluie, H. (2019). Convolutions on the sphere: Commutation with differential operators. *GEM—International Journal on Geomathematics*, *10*(2), 9. https://doi.org/10.1007/s13137-019-0123-9

Aluie, H., Hecht, M., & Vallis, G. K. (2018). Mapping the energy cascade in the North Atlantic Ocean: The coarse-graining approach. *Journal of Physical Oceanography*, *48*(2), 225–244. https://doi.org/10.1175/JPO-D-17-0100.1

Danilov, S., Juricke, S., Nowak, E. A. K., & Wang, Q. (2024). Extracting spatial spectra using coarse-graining based on implicit filters. *ESS Open Archive*. (under review). https://doi.org/10.22541/essoar.169111691.14930425/v1

Danilov, S., Sidorenko, D., Wang, Q., & Jung, T. (2017). The finite-volume sea ice–ocean model (FESOM2). *Geoscientific Model Development*, *10*(2), 765–789. https://doi.org/10.5194/gmd-10-765-2017

Danilov, S., Wang, Q., Timmermann, R., Iakovlev, N., Sidorenko, D., Kimmritz, M., et al. (2015). Finite-element sea ice model (FESIM), version 2. *Geoscientific Model Development*, *8*(6), 1747–1761. https://doi.org/10.5194/gmd-8-1747-2015

Ferrari, R., & Wunsch, C. (2009). Ocean circulation kinetic energy: Reservoirs, sources, and sinks. *Annual Review of Fluid Mechanics*, *41*(1), 253–282. https://doi.org/10.1146/annurev.fluid.40.111406.102139

Hersbach, H., Bell, B., Berrisford, P., Hirahara, S., Horányi, A., Muñoz-Sabater, J., et al. (2020). The ERA5 global reanalysis. *Quarterly Journal of the Royal Meteorological Society*, *146*(730), 1999–2049. https://doi.org/10.1002/qj.3803

Karcher, M. J., & Oberhuber, J. M. (2002). Pathways and modification of the upper and intermediate waters of the Arctic Ocean. *Journal of Geophysical Research*, *107*(C6), 2-1–2-13. https://doi.org/10.1029/2000JC000530

Kawaguchi, Y., Itoh, M., & Nishino, S. (2012). Detailed survey of a large baroclinic eddy with extremely high temperatures in the western Canada basin. *Deep Sea Research Part I: Oceanographic Research Papers*, *66*, 90–102. https://doi.org/10.1016/j.dsr.2012.04.006

Klein, P., Hua, B. L., Lapeyre, G., Capet, X., Gentil, S. L., & Sasaki, H. (2008). Upper ocean turbulence from high-resolution 3d simulations. *Journal of Physical Oceanography*, *38*(8), 1748–1763. https://doi.org/10.1175/2007JPO3773.1

Koldunov, N. V., Danilov, S., Sidorenko, D., Hutter, N., Losch, M., Goessling, H., et al. (2019). Fast EVP solutions in a high-resolution sea ice model. *Journal of Advances in Modeling Earth Systems*, *11*(5), 1269–1284. https://doi.org/10.1029/2018MS001485

Kozlov, I. E., Artamonova, A. V., Manucharyan, G. E., & Kubryakov, A. A. (2019). Eddies in the Western Arctic Ocean from spaceborne SAR observations over open ocean and marginal ice zones. *Journal of Geophysical Research: Oceans*, *124*(9), 6601–6616. https://doi.org/10.1029/2019JC015113

Liu, C., Wang, Q., & Danilov, E. A. S. (2024). Spatial scales of kinetic energy in the Arctic Ocean [Dataset]. *Zenodo*. https://doi.org/10.5281/zenodo.7895619

Manley, T. O., & Hunkins, K. (1985). Mesoscale eddies of the Arctic Ocean. *Journal of Geophysical Research*, *90*(C3), 4911–4930. https://doi.org/10.1029/JC090iC03p04911

Manucharyan, G. E., & Thompson, A. F. (2022). Heavy footprints of upper-ocean eddies on weakened Arctic Sea ice in the marginal ice zones. *Nature Communications*, *13*(1), 2147. https://doi.org/10.1038/s41467-022-29663-0

Meneghello, G., Marshall, J., Lique, C., Isachsen, P. E., Doddridge, E., Campin, J.-M., et al. (2021). Genesis and decay of mesoscale baroclinic eddies in the seasonally ice-covered interior Arctic Ocean. *Journal of Physical Oceanography*, *51*(1), 115–129. https://doi.org/10.1175/JPO-D-20-0054.1

Nurser, A. J. G., & Bacon, S. (2014). The rossby radius in the Arctic Ocean. *Ocean Science*, *10*(6), 967–975. https://doi.org/10.5194/os-10-967-2014

Pickart, R. S., Weingartner, T. J., Pratt, L. J., Zimmermann, S., & Torres, D. J. (2005). Flow of winter-transformed Pacific water into the western Arctic. *Deep Sea Research Part II: Topical Studies in Oceanography*, *52*(24), 3175–3198. (The Western Arctic Shelf-Basin Interactions (SBI) Project). https://doi.org/10.1016/j.dsr2.2005.10.009

Pnyushkov, A., Polyakov, I. V., Padman, L., & Nguyen, A. T. (2018). Structure and dynamics of mesoscale eddies over the Laptev Sea continental slope in the Arctic Ocean. *Ocean Science*, *14*(5), 1329–1347. https://doi.org/10.5194/os-14-1329-2018

Qiu, B., Chen, S., Klein, P., Wang, J., Torres, H., Fu, L.-L., & Menemenlis, D. (2018). Seasonality in transition scale from balanced to unbalanced motions in the world ocean. *Journal of Physical Oceanography*, *48*(3), 591–605. https://doi.org/10.1175/JPO-D-17-0169.1

Rai, S., Hecht, M., Maltrud, M., & Aluie, H. (2021). Scale of oceanic eddy killing by wind from global satellite observations. *Science Advances*, *7*(28), eabf4920. https://doi.org/10.1126/sciadv.abf4920

Regan, H., Lique, C., Talandier, C., & Meneghello, G. (2020). Response of total and eddy kinetic energy to the recent spinup of the beaufort gyre. *Journal of Physical Oceanography*, *50*(3), 575–594. https://doi.org/10.1175/JPO-D-19-0234.1

Rudels, B. (2012). Arctic Ocean circulation and variability: Advection and external forcing encounter constraints and local processes. *Ocean Science*, *8*(2), 261–286. https://doi.org/10.5194/os-8-261-2012

Rudels, B., Anderson, L. G., & Jones, E. P. (1996). Formation and evolution of the surface mixed layer and halocline of the Arctic Ocean. *Journal of Geophysical Research*, *101*(C4), 8807–8821. https://doi.org/10.1029/96JC00143

Sadek, M., & Aluie, H. (2018). Extracting the spectrum of a flow by spatial filtering. *Physical Review Fluids*, *3*(12), 124610. https://doi.org/10.1103/PhysRevFluids.3.124610

Scholz, P., Sidorenko, D., Danilov, S., Wang, Q., Koldunov, N., Sein, D., & Jung, T. (2022). Assessment of the finite-volume sea ice–ocean model (FESOM2.0)—Part 2: Partial bottom cells, embedded sea ice and vertical mixing library CVMix. *Geoscientific Model Development*, *15*(2), 335–363. https://doi.org/10.5194/gmd-15-335-2022

Scholz, P., Sidorenko, D., Gurses, O., Danilov, S., Koldunov, N., Wang, Q., et al. (2019). Assessment of the finite-volume sea ice-ocean model (FESOM2.0)—Part 1: Description of selected key model elements and comparison to its predecessor version. *Geoscientific Model Development*, *12*(11), 4875–4899. https://doi.org/10.5194/gmd-12-4875-2019

Schubert, R., Gula, J., Greatbatch, R. J., Baschek, B., & Biastoch, A. (2020). The submesoscale kinetic energy cascade: Mesoscale absorption of submesoscale mixed layer eddies and frontal downscale fluxes. *Journal of Physical Oceanography*, *50*(9), 2573–2589. https://doi.org/10.1175/JPO-D-19-0311.1

Spall, M. A. (2013). On the circulation of Atlantic water in the Arctic Ocean. *Journal of Physical Oceanography*, *43*(11), 2352–2371. https://doi.org/10.1175/JPO-D-13-079.1

Spall, M. A., Pickart, R. S., Fratantoni, P. S., & Plueddemann, A. J. (2008). Western arctic shelfbreak eddies: Formation and transport. *Journal of Physical Oceanography*, *38*(8), 1644–1668. https://doi.org/10.1175/2007JPO3829.1

Steele, M., Morley, R., & Ermold, W. (2001). PHC: A global ocean hydrography with a high-quality Arctic Ocean. *Journal of Climate*, *14*(9), 2079–2087. https://doi.org/10.1175/1520-0442(2001)014⟨2079:PAGOHW⟩2.0.CO;2

Storer, B. A., Buzzicotti, M., Khatri, H., Griffies, S. M., & Aluie, H. (2022). Global energy spectrum of the general oceanic circulation. *Nature Communications*, *13*(1), 5314. https://doi.org/10.1038/s41467-022-33031-3

Timmermans, M.-L., & Marshall, J. (2020). Understanding Arctic Ocean circulation: A review of ocean dynamics in a changing climate. *Journal of Geophysical Research: Oceans*, *125*(4), e2018JC014378. https://doi.org/10.1029/2018JC014378

Timmermans, M.-L., Toole, J., Proshutinsky, A., Krishfield, R., & Plueddemann, A. (2008). Eddies in the Canada basin, Arctic Ocean, observed from ice-tethered profilers. *Journal of Physical Oceanography*, *38*(1), 133–145. https://doi.org/10.1175/2007JPO3782.1

Uchida, T., Abernathey, R., & Smith, S. (2017). Seasonality of eddy kinetic energy in an eddy permitting global climate model. *Ocean Modelling*, *118*, 41–58. https://doi.org/10.1016/j.ocemod.2017.08.006

von Appen, W.-J., Baumann, T. M., Janout, M., Koldunov, N., Lenn, Y.-D., Pickart, R. S., et al. (2022). Eddies and the distribution of eddy kinetic energy in the Arctic Ocean. *Oceanography*, *35*(3–4), 42–51. https://doi.org/10.5670/oceanog.2022.122

von Appen, W.-J., Schauer, U., Hattermann, T., & Beszczynska-Möller, A. (2016). Seasonal cycle of mesoscale instability of the west spitsbergen current. *Journal of Physical Oceanography*, *46*(4), 1231–1254. https://doi.org/10.1175/JPO-D-15-0184.1

Wang, Q., & Danilov, S. (2022). A synthesis of the upper Arctic Ocean circulation during 2000–2019: Understanding the roles of wind forcing and sea ice decline. *Frontiers in Marine Science*, *9*. https://doi.org/10.3389/fmars.2022.863204

Wang, Q., Koldunov, N. V., Danilov, S., Sidorenko, D., Wekerle, C., Scholz, P., et al. (2020). Eddy kinetic energy in the Arctic Ocean from a global simulation with a 1-km Arctic. *Geophysical Research Letters*, *47*(14), e2020GL088550. https://doi.org/10.1029/2020GL088550

Wang, Q., Shu, Q., Bozec, A., Chassignet, E. P., Fogli, P. G., Fox-Kemper, B., et al. (2024). Impact of increased resolution on Arctic Ocean simulations in ocean model intercomparison project phase 2 (OMIP-2). *Geoscientific Model Development*, *17*(1), 347–379. https://doi.org/10.5194/gmd-17-347-2024

Watanabe, E., Onodera, J., Harada, N., Honda, M. C., Kimoto, K., Kikuchi, T., et al. (2014). Enhanced role of eddies in the Arctic marine biological pump. *Nature Communications*, *5*(1), 3950. https://doi.org/10.1038/ncomms4950

Wekerle, C., Hattermann, T., Wang, Q., Crews, L., von Appen, W.-J., & Danilov, S. (2020). Properties and dynamics of mesoscale eddies in Fram Strait from a comparison between two high-resolution ocean–sea ice models. *Ocean Science*, *16*(5), 1225–1246. https://doi.org/10.5194/os-16-1225-2020

Wekerle, C., Wang, Q., von Appen, W.-J., Danilov, S., Schourup-Kristensen, V., & Jung, T. (2017). Eddy-resolving simulation of the Atlantic water circulation in the Fram Strait with focus on the seasonal cycle. *Journal of Geophysical Research: Oceans*, *122*(11), 8385–8405. https://doi.org/10.1002/2017JC012974

Woodgate, R. A., Aagaard, K., Muench, R. D., Gunn, J., Björk, G., Rudels, B., et al. (2001). The Arctic Ocean boundary current along the Eurasian slope and the adjacent Lomonosov Ridge: Water mass properties, transports and transformations from moored instruments. *Deep Sea Research Part I: Oceanographic Research Papers*, *48*(8), 1757–1792. https://doi.org/10.1016/S0967-0637(00)00091-1

Zhao, M., & Timmermans, M.-L. (2015). Vertical scales and dynamics of eddies in the Arctic Ocean's Canada basin. *Journal of Geophysical Research: Oceans*, *120*(12), 8195–8209. https://doi.org/10.1002/2015JC011251

Zhao, M., Timmermans, M.-L., Cole, S., Krishfield, R., Proshutinsky, A., & Toole, J. (2014). Characterizing the eddy field in the Arctic Ocean halocline. *Journal of Geophysical Research: Oceans*, *119*(12), 8800–8817. https://doi.org/10.1002/2014JC010488

Zhao, M., Timmermans, M.-L., Cole, S., Krishfield, R., & Toole, J. (2016). Evolution of the eddy field in the Arctic Ocean's Canada basin, 2005–2015. *Geophysical Research Letters*, *43*(15), 8106–8114. https://doi.org/10.1002/2016GL069671

Erratum

The originally published version of this article contained a typographical error. Coauthor Nikolay Koldonov's name should be spelled Nikolay Koldunov. The error has been corrected, and this may be considered the authoritative version of record.